

HOPPS: Hardware-Aware Optimal Phase Polynomial Synthesis with Blockwise Optimization for Quantum Circuits

Xinpeng Li

*Dept. of Computer and Data Science
Case Western Reserve University
Cleveland, US
xxl1337@case.edu*

Ji Liu

*Mathematics and Computer Science Division
Argonne National Laboratory
Lemont, US
ji.liu@anl.gov*

Shuai Xu

*Dept. of Computer and Data Science
Case Western Reserve University
Cleveland, US
ssx214@case.edu*

Paul Hovland

*Mathematics and Computer Science Division
Argonne National Laboratory
Lemont, US
hovland@anl.gov*

Vipin Chaudhary

*Dept. of Computer and Data Science
Case Western Reserve University
Cleveland, US
vxc204@case.edu*

Abstract—Blocks composed of $\{\text{CNOT}, R_z\}$ are ubiquitous in modern quantum applications, notably in circuits such as QAOA ansatzes and quantum adders. After compilation, many of them exhibit large CNOT counts or depths, which lowers fidelity. Therefore, we introduce HOPPS: a SAT-based hardware-aware optimal phase polynomial synthesis algorithm that could generate $\{\text{CNOT}, R_z\}$ blocks with CNOT count or depth optimality.

Sometime $\{\text{CNOT}, R_z\}$ blocks are large, such as in QAOA ansatzes, HOPPS’s pursuit of optimality limits its scalability. To address this issue, we introduce an iterative blockwise optimization strategy: large circuits are partitioned into smaller blocks, each block is optimally refined, and the process is repeated for several iterations.

Empirical results show that HOPPS is more efficient comparing with existing near-optimal synthesis tools. Used as a peephole optimizer, HOPPS reduces the CNOT count by up to 50.0% and the CNOT depth by up to 57.1% under OLSQ. For large QAOA circuit, after mapping by Qiskit, circuit can be reduced CNOT count and depth by up to 44.4% and 42.4% by our iterative blockwise optimization.

Index Terms—Phase Polynomial, Quantum Circuit Synthesis, Quantum Circuit Optimization.

I. INTRODUCTION

NISQ quantum devices, both near-term devices [1], [2] and long-term scalable quantum architectures [3], [4], are constrained by limited qubit connectivity, permitting two-qubit gates only between physically connected qubits. Additionally, two-qubit gates tend to have higher error rates and longer durations. As a result, increasing their count or depth reduces overall circuit fidelity. Therefore, optimizing the number and depth of two-qubit operations is necessary for NISQ quantum devices [5], [6].

Among quantum applications, circuits composed of $\{\text{CNOT}, R_z(\theta)\}$ gates are frequently used in designs such as the Quantum Approximate Optimization Algorithm

(QAOA) [7], quantum adders [8], and the quantum Fourier transform (QFT) [9]. Fortunately, such circuits can be efficiently encoded as low-degree polynomials over the finite field \mathbb{F}_2 using a phase polynomial representation [10], [11]. Unlike unitary matrix representations, which require $O(2^{2n})$ memory to store, the phase polynomial representation scales linearly with the number of qubits, i.e., $O(n^2)$. This compact representation facilitates both phase polynomial circuit synthesis [12]–[14] and circuit verification [15].

In this work, we focus on phase polynomial circuit synthesis, which is the process of generating a $\{\text{CNOT}, R_z(\theta)\}$ circuit from its phase polynomial representation. We observe that existing studies have explored both heuristic and optimal solutions for logical-level circuits [12], [14], as well as heuristic methods for physical-level circuits [13], [16], [17]. However optimal synthesis under arbitrary hardware constraints remains unaddressed. This motivates us to introduce an algorithm for Hardware-Aware Optimal Phase Polynomial Synthesis, called **HOPPS**.

Because phase polynomial synthesis operates entirely in a binary encoding, SAT is well-suited to circuit synthesis. On NISQ hardware, CNOT gates are error-prone and have relatively long durations comparing with $R_z(\theta)$, we provide both CNOT count and depth optimal synthesis results. We claim HOPPS can also provide doubly optimal based on one of metrics. For example, a CNOT-based doubly optimal solution not only minimizes the CNOT count but also achieves the minimal CNOT depth under that optimal CNOT count.

While HOPPS provides optimal physical circuits, it faces scalability challenges. Therefore, we explore how optimal solutions can be practically leveraged. One key application of HOPPS is peephole optimization on mapped circuits. However, in some cases—such as QAOA circuits, which are

almost entirely composed of $\{\text{CNOT}, R_z(\theta)\}$ gates—the block may be too large for direct optimization. To address this, we propose an **Iterative Blockwise Optimization** approach: repeating (1) partitioning circuit into smaller blocks (2) optimizing blocks using HOPPS. Fortunately, the independence of blocks enables efficient **parallel execution** for each iteration.

Our main contributions are summarized as follows:

- We propose a SAT-based algorithm, named HOPPS, that synthesizes doubly optimal CNOT count or CNOT depth $\{\text{CNOT}, R_z(\theta)\}$ circuits under hardware topology.
- We introduce an iterative blockwise optimization strategy for large-scale $\{\text{CNOT}, R_z(\theta)\}$ circuits.
- We propose a parallel framework that enables iterative blockwise optimization to run efficiently on HPC systems.

The remainder of this paper is organized as follows. Section II provides the necessary background. In Section III we explain the synthesis problem and our objective. Section IV presents our SAT-based synthesis algorithm HOPPS. Section V presents the peephole optimization, iterative blockwise optimization strategies and their parallel implementation. Section VI presents some related work. Experimental results are reported in Section VII. Finally, Section VIII discusses the benefits of using HOPPS, and Section IX summarizes our findings and outlines directions for future work.

II. BACKGROUND

A. Phase Polynomial Representation

The Phase Polynomial Representation is an alternative representation for a quantum circuit composed exclusively of gates from the set $\{\text{CNOT}, R_z(\theta)\}$. When an n -qubit circuit is restricted to these gates, it can be expressed by using the circuit-polynomial correspondence [10], consisting of a phase polynomial function $p(\cdot)$ and a linear reversible function $g(\cdot)$. The action on a basis state $|x\rangle$ can be written as

$$|x\rangle \mapsto e^{2\pi i p(x)} |g(x)\rangle. \quad (1)$$

Here, the phase polynomial is given by

$$p(x) = \sum_{i=0}^{2^n-1} \theta_i f_i(x). \quad (2)$$

First, in $p(x)$, each $f_i(x)$ is a linear Boolean function, $f_i : \mathbb{F}_2^n \rightarrow \mathbb{F}_2$, thus can be represented as a binary coefficient vector $\mathbf{t}^{(i)} = (t_0^{(i)}, t_1^{(i)}, \dots, t_n^{(i)}) \in \mathbb{F}_2^n$ and written as

$$f_i(x) = \mathbf{t}^{(i)} \cdot x = t_0^{(i)} x_0 \oplus t_1^{(i)} x_1 \oplus \dots \oplus t_n^{(i)} x_n. \quad (3)$$

We collect all these vectors from f_0, \dots, f_{n-1} form a set of binary vectors $T = \{\mathbf{t}^{(0)}, \dots, \mathbf{t}^{(n-1)}\}$, which is also referred to as the “parity table” [12]. In the Eq. 2, each boolean function $f_i(x)$ is associated with a corresponding parameter θ_i , collectively forming the parameter set $\Theta = \{\theta_0, \dots, \theta_{n-1}\}$. The sets Θ and T are in one-to-one correspondence.

Second, the function $g(x)$, $g : \mathbb{F}_2^n \rightarrow \mathbb{F}_2^n$, in the Eq. 1 can also be expressed as a vector-valued function $g(x) =$

$(g_0(x), g_1(x), \dots, g_{n-1}(x))$, where each component $g_j(x)$ is a linear Boolean function. Each $g_j(x)$ is defined by a coefficient vector $\mathbf{g}^{(j)} = (g_0^{(j)}, g_1^{(j)}, \dots, g_n^{(j)})$ and is written as

$$g_j(x) = \mathbf{g}^{(j)} \cdot x = g_0^{(j)} x_0 \oplus g_1^{(j)} x_1 \oplus \dots \oplus g_n^{(j)} x_n. \quad (4)$$

Similarly, the linear reversible function $g(x)$ can be represented by a binary matrix G , where each row corresponds to the coefficient vector $\mathbf{g}^{(j)}$ of the Boolean function $g_j(x)$. That is, the transformation $g(x)$ is realized through matrix-vector multiplication:

$$g(x) = Gx \pmod{2},$$

where $G \in \mathbb{F}_2^{n \times n}$ is an invertible binary matrix, also known as a parity matrix.

In summary, a circuit composed of gates from the set $\{\text{CNOT}, R_z(\theta)\}$ can be succinctly represented by a parity table T , parameter set Θ and a parity matrix G .

B. Phase Polynomial Circuit Representation Extraction

Given a circuit, we do not have to extract Phase Polynomial Representation writing in Eq. 1. For an n -qubit circuit, it begins with an initial state

$$|x\rangle = |x_0\rangle |x_1\rangle \dots |x_{n-1}\rangle,$$

where each qubit is initialized independently. When a CNOT is applied, it will perform:

$$\text{CNOT} : |x_i\rangle |x_j\rangle \mapsto |x_i\rangle |x_i \oplus x_j\rangle.$$

This process can be efficiently tracked parity of the circuit P called *circuit parity*. Because P changes over time, we write $P_{k,i,j}$ for the entry in row i and column j at time step k . The initial circuit parity P_0 is typically the identity matrix. A CNOT gate performs an XOR between two row vectors of P , replacing one of the rows, as illustrated in Fig. 1(d). We traverse the circuit, updating the circuit parity under each CNOT; whenever we encounter an $R_z(\theta)$ on the i th qubit, we record the current circuit parity (the i th row of the parity table) into T . When the process completes, the final circuit parity is G . We provide an example in Fig. 1 (a).

C. Phase Polynomial Synthesis

Phase polynomial synthesis is the reverse process of extracting a phase polynomial representation from a circuit. It involves reconstructing a quantum circuit from: 1) a phase polynomial parity table T ; 2) a parameter set Θ ; and 3) a linear transformation parity matrix G . During synthesis, we continuously add CNOT gates to match each $t_i(x)$ and matrix G finally. The $R_z(\theta_i)$ gates are placed at the circuit positions corresponding to $t_i(x)$.

Example. To illustrate the synthesis process, we provide an example of a three-qubit QAOA cost layer synthesis. The parity table T and the final (target) circuit parity matrix G are

$$T = \begin{bmatrix} 1 & 0 & 1 \\ 1 & 1 & 0 \\ 0 & 1 & 1 \end{bmatrix} \quad G = \begin{bmatrix} 1 & 0 & 0 \\ 0 & 0 & 1 \\ 0 & 1 & 0 \end{bmatrix}.$$

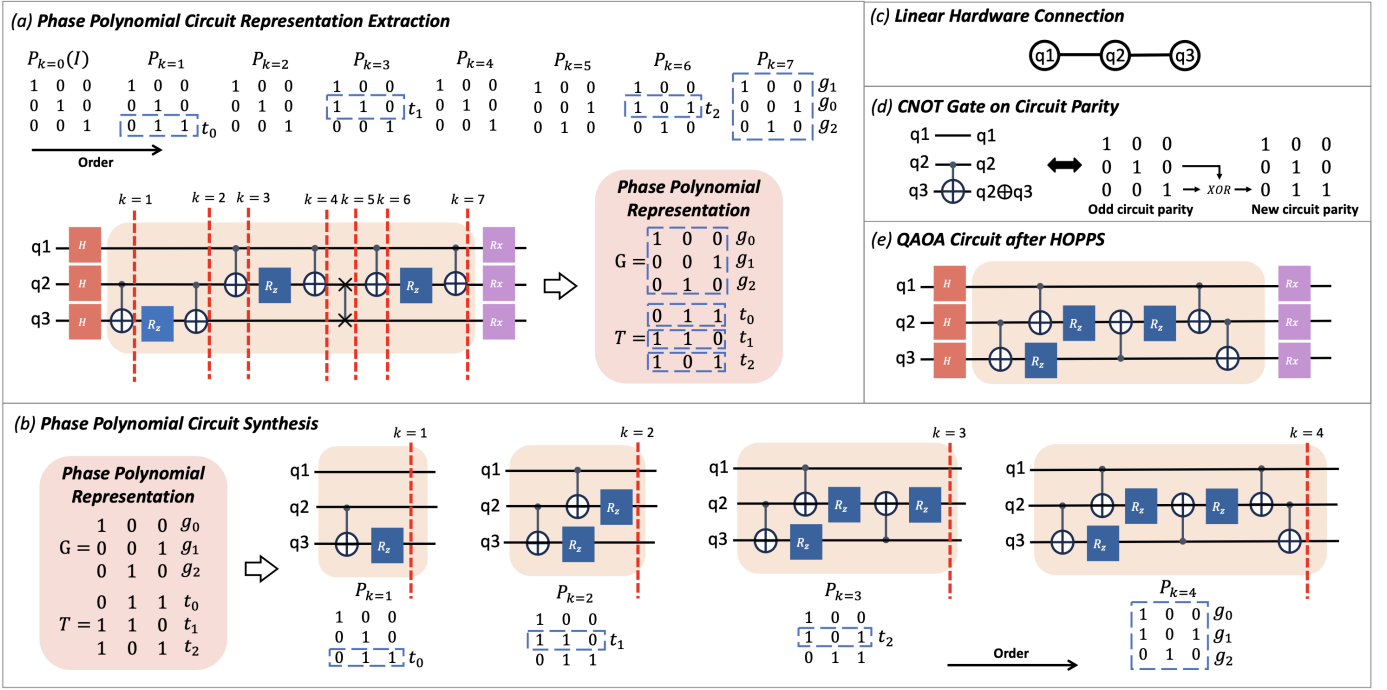


Fig. 1: Explanation of Phase Polynomial Representation and Synthesis. **(a)** Extracting the phase polynomial representation from a QAOA circuit. The circuit is scanned from beginning to end, starting with an identity matrix. Each CNOT gate updates the circuit’s parity matrix. When an $R_z(\theta)$ gate is encountered, the parity vector associated with that qubit is recorded and stored in the table T . After processing the entire circuit, only the final circuit parity matrix G and the table T are retained. **(b)** Synthesizing a circuit from the phase polynomial representation. CNOT gates are iteratively added, and the parity matrix is updated accordingly. When a qubit’s parity vector matches one in T , an $R_z(\theta)$ gate is inserted. After all $t \in T$ are found, we continuously add CNOT gates to make the parity match G . *Note: This process is not used in this paper; it is provided solely to aid in understanding the problem.* **(c)** Linear hardware topology. The circuits in (a), (b), and (e) obey this constraint, meaning that qubit 1 and qubit 3 cannot be directly connected. **(d)** Effect of a CNOT gate on circuit parity. A CNOT operation updates the parity matrix by applying a bitwise XOR between the control and target vectors, replacing the control vector with the result. **(e)** Optimal solution for the QAOA circuit in (a) under the hardware topology in (c).

For convenience, we refer to each row in the parity table T as a *term parity*, since it corresponds to a term in the phase polynomial $p(x)$.

As shown in Fig. 1 (b), the circuit is initialized with the identity parity matrix. In order to implement the first term parity $t_0 = [0, 1, 1]$ on qubit q_3 , a CNOT gate is applied with control on q_2 and target on q_3 . This corresponds to updating $P_{0,3,j}$ by performing a XOR with $P_{0,2,j}$ if $P_{0,2,j} = 1$ for all $0 \leq j < 3$. As a result, the third row of the matrix becomes equal to t_0 , and we can apply R_z on it. We continue adding CNOT gates until all $t \in T$ are applied as $R_z(\theta)$ gates in the circuit. Note that each term parity should be synthesized only once, and the order of synthesis does not affect correctness. After finishing synthesis T , we need some CNOT gates to convert circuit parity to matrix G . Finally, we assign θ_i to their corresponding term parity positions. At this point, the synthesis process terminates. Synthesizing such circuits is an NP-complete problem [18].

We emphasize that a single synthesized circuit is reused for multiple parameter sets Θ . The core of the synthesis process is to make the circuit parity match every term parity in T at

least once and the final parity matrix G in the end.

D. SAT

SAT (Boolean satisfiability) employs a solver to decide if a satisfying Boolean assignment exists for a specified set of constraints. The given problem is encoded as boolean variables and boolean formulas using operators AND, OR, and NOT to constrain variables. In this paper, we encode phase polynomial synthesis—which can naturally be expressed in binary—as a problem over Boolean variables and constraints.

To obtain an optimal solution, the SAT solver performs incremental satisfiability checks: it starts from a known lower bound and progressively enlarges the search space. The first instance that proves satisfiable yields an optimal solution.

E. Hardware Restriction and SWAP Based Mapper

On real Noisy Intermediate-Scale Quantum (NISQ) devices, two-qubit gates are often limited to specific pairs of physical qubits, depending on the device’s connectivity topology. We can model this topology as a graph $CP = (Q, E)$, where each node $q_i \in Q$ represents a physical qubit and each edge $e \in E$

indicates that a two-qubit gate can be directly applied between the connected qubits. This graph is called the coupling map.

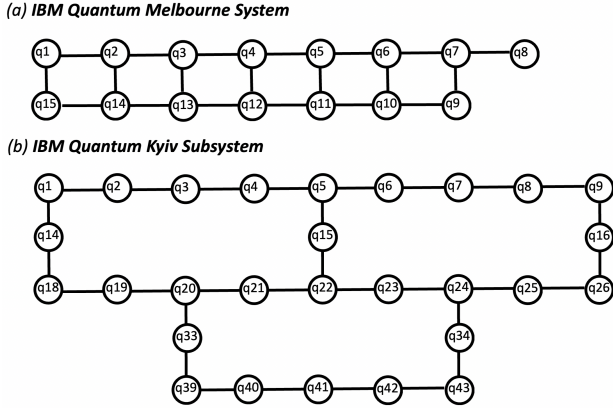


Fig. 2: Overview of the coupling map (qubit-connectivity topology) for the `ibmq_melbourne` system and `ibmq_kyiv` subsystem. Nodes represent physical qubits, and edges indicate allowed two-qubit gate operations on two physical qubits.

Example. Fig. 2 shows the coupling map CP for `ibmq_melbourne` system and `ibmq_kyiv` subsystem. As seen in the figure, the connectivity is limited—many qubits are connected in a nearly linear or sparse topology.

To apply a two-qubit gate between non-adjacent qubit pairs, traditional compilation techniques insert SWAP gates to move qubits closer until the desired pair becomes adjacent. This process is commonly referred to as *layout synthesis* [19] or *qubit mapping* [20]. SWAP operations are expensive, typically decomposing into three CNOT gates; therefore, the mapping procedure should minimize the number of required SWAPs.

III. HARDWARE-AWARE OPTIMAL PHASE POLYNOMIAL SYNTHESIS

The key novelty of our phase-polynomial synthesis is twofold: *hardware-aware*, *optimality*. We elaborate on these objectives below.

A. Hardware-Aware Synthesis

Hardware-aware synthesis requires that inserted CNOT gates respect the hardware topology, which increases the complexity of the synthesis process. In Fig. 1(e), we show the result of applying hardware-aware synthesis to the QAOA circuit from Fig. 1(a) under a linear topology in Fig. 1(c).

B. Optimal Synthesis

In quantum circuit synthesis, CNOT count and CNOT depth are two commonly used metrics, due to two-qubit gates are error-prone and have relatively long durations. However, a circuit that is optimal in terms of CNOT count is not necessarily optimal in depth, and vice versa.

Nevertheless, we propose the notion of “doubly optimal synthesis”. This refers to cases where, under an optimal CNOT count, the CNOT depth is also minimized, and conversely,

under an optimal CNOT depth, the CNOT count is also minimized. We refer to these two scenarios as **CNOT-based doubly optimal** and **depth-based doubly optimal**, respectively.

IV. HOPPS: AN SAT-BASED {CNOT, RZ} CIRCUIT SYNTHESIS ALGORITHM

The HOPPS algorithm is a SAT-based approach that takes the initial parity matrix I , final parity matrix G , parity table T , term rotation angles Θ , and the coupling map graph CP as input. It outputs a quantum circuit qc . The algorithm supports two optimization objectives: minimizing the total CNOT count (HOPPS-CNOT) or minimizing the CNOT depth (HOPPS-Depth). Both of them can be doubly optimized. Since both objectives share the same variable encoding, but differ in constraints, we first introduce the common variables and constraints, followed by a description of the differences.

A. Common Variable Encoding

The primary variables are derived from two aspects:

- **Encoding CNOT gates:** For each edge $e(q_i, q_j)$ in the coupling map, two possible CNOT gates can be applied—one with q_i as the control and q_j as the target, and the other with q_j as the control and q_i as the target. We denote \vec{e} as a directed edge in the directed coupling map \vec{CP} , and define a binary variable $cnot_{k,\vec{e}}$ to indicate whether a CNOT gate is applied at time step k along the directed edge \vec{e} .
- **Encoding circuit parity:** To track how the circuit parity evolves with CNOT gates applied just like in Fig. 1 (b), we define a three-dimensional binary matrix $P_{k,i,j}$, where k represents the time step and i, j are row and column indices indicating the circuit parity state at that moment. At each time step k , the circuit parity is updated based on the CNOT operations applied, represented by the vector $[cnot_{k,\vec{e}} \mid \vec{e} \in \vec{E}]$.

B. Common Constraints

1) *Initial Final Circuit Parity Matrix:* First, we constrain the initial and final circuit parity. Assuming the initial parity matrix is represented by matrix I and the final by matrix G , the constraints are as follows.

$$\bigvee_{i,j} I_{i,j} = P_{0,i,j} \quad (5)$$

$$\bigvee_{i,j} G_{i,j} = P_{n_{\text{term}},i,j} \quad (6)$$

2) *Parity Table:* Second, our goal is to find all n_{term} term parities in the circuit parity. For each term parity t_{nt} , there must exist at least one row in the circuit parity that matches them:

$$\bigvee_{nt} \exists_{k,i} \text{AND}(t_{nt,j} = P_{k,i,j}). \quad (7)$$

3) *CNOT Dependence*: Third, the circuit parity P_{k+1} is updated when a CNOT gate is applied at the time step k . Suppose a CNOT gate is inserted with a control qubit q_i and a target qubit q_j at time k . The circuit parity P_{k+1} 's row i remains unchanged, while the row j is updated by performing a bitwise XOR with the row i .

We can use two logical implies (\Rightarrow) to model the XOR operation. Assuming a CNOT is applied on the directed edge $\vec{e} = [q_m, q_n]$, if $P_{k,m,i}$ is true, then $P_{k+1,n,i}$ must differ from $P_{k,n,i}$; otherwise, $P_{k+1,n,i}$ should remain unchanged. The logical constraints are expressed as follows.

$$\bigvee_{k,\vec{e},j} (\text{AND}(cnot_{k,\vec{e}}, P_{k,\vec{e}[0],j}) \Rightarrow P_{k+1,\vec{e}[1],j} \neq P_{k,\vec{e}[1],j}) \quad (8)$$

$$\bigvee_{k,\vec{e},j} (\text{AND}(cnot_{k,\vec{e}}, \neg P_{k,\vec{e}[0],j}) \Rightarrow P_{k+1,\vec{e}[1],j} = P_{k,\vec{e}[1],j}) \quad (9)$$

$$\bigvee_{k,i,j} (\text{AND}(\neg cnot_{k,\vec{e}} \mid q_i \in \vec{e}, \vec{e} \in \vec{E}) \Rightarrow P_{k+1,i,j} = P_{k,i,j}) \quad (10)$$

C. Constraints for CNOT Optimal

For CNOT count optimal, we restrict each $cnot_{k,e}$ such that at most one CNOT operation can occur across all time steps $0 \leq k < K$. This restriction is enforced by applying `AtLeast` and `AtMost` constraints.

$$\bigvee_k (\text{AtLeast}(\{cnot_{k,\vec{e}} \mid \vec{e} \in \vec{E}\}, 1)) \quad (11)$$

$$\bigvee_k (\text{AtMost}(\{cnot_{k,\vec{e}} \mid \vec{e} \in \vec{E}\}, 1)) \quad (12)$$

D. Constraints for CNOT-Based Doubly Optimal

To achieve CNOT-based doubly optimal synthesis, we first minimize the number of CNOT gates to obtain optimal CNOT count. Then, given this optimal CNOT count, we search for the minimal CNOT depth by incrementally adding constraints. To finish the second process, we firstly introduce two auxiliary binary variable matrices:

- **Mapping Gate to Layer**: Define a binary matrix $D_{k,l}$ where $0 \leq k < K$ and $0 \leq l < K$. $D_{k,l} = 1$ indicates that the CNOT gate $cnot_{k,\vec{e}}$ at time step k is assigned to layer l .
- **Mapping Layer to CNOT Gate**: Define another binary matrix $L_{l,\vec{e}}$, where $L_{l,\vec{e}} = 1$ denotes that the CNOT gate acting on edge \vec{e} appears in layer l .

1) *Valid Layer Assignment*: Each CNOT gate must be assigned to exactly one layer, which leads to the following constraints:

$$\bigvee_k \text{AtLeast}(\{D_{k,l} \mid 0 \leq l < K\}, 1) \quad (13)$$

$$\bigvee_k \text{AtMost}(\{D_{k,l} \mid 0 \leq l < K\}, 1) \quad (14)$$

2) *Reduce the Searching Space*: To enable efficient search, we enforce temporal continuity within each layer by disallowing alternating or skipping time steps in that layer. That is, if a CNOT gate is assigned to layer l at time k , then the next gate assigned to layer l should be at time $k+1$ or there is not gates assigned to layer l after time k . We express this continuity constraint as:

$$\bigvee_{k < K-1, l} (D_{k,l} \Rightarrow \text{OR}(D_{k+1,l}, \text{AND}(\{\neg D_{k+i,l} \mid 1 \leq i < K-k\})) \quad (15)$$

To avoid permutation search over layer assignments, we constrain the layer indices to increase monotonically with time. That is, if a CNOT gate at time step k is assigned to layer l_k , and the next gate at $k+1$ is assigned to l_{k+1} , then $l_k \leq l_{k+1}$. This constraint is enforced as:

$$\bigvee_{k < K-1, l} (D_{k,l} \Rightarrow \text{AND}(\{\neg D_{k+i,l-j} \mid 1 \leq i < K-k; 0 \leq j < l\})) \quad (16)$$

3) *Valid Layer Topology*: To ensure that the CNOT gates in each layer conform to the hardware topology, we use $L_{l,\vec{e}}$ to indicate whether a CNOT gate acting on edge \vec{e} appears in layer l . We have:

$$\bigvee_{l,\vec{e} \in \vec{E}} (L_{l,\vec{e}} = \text{OR}(\{\text{AND}(D_{k,l}, cnot_{k,\vec{e}}) \mid 0 \leq k < K\})) \quad (17)$$

Then, we restrict on each layer there are no two CNOTs interfere on the same qubit simultaneously:

$$\bigvee_{l,i} (\text{AtMost}(\{L_{l,\vec{e}} \mid q_i \in \vec{e}; \vec{e} \in \vec{E}\}, 1)) \quad (18)$$

4) *Control the Depth*: To control the solution circuit adapts depth d , we add the following constraints:

$$\bigvee_{k,l \geq d} \neg D_{k,l} \quad (19)$$

This enforces that no CNOT gate is assigned to a layer index $l \geq d$. Then the solver is forced to find a solution within the desired depth bound.

E. Constraints for Depth Optimal

1) *Valid Layer*: For CNOT depth optimal, we impose two constraints: 1) no two CNOT gates may act on the same physical qubit at the same time step k , and 2) at least one CNOT gate must be scheduled at each time step. These constraints are encoded using `AtLeast` and `AtMost` as following:

$$\bigvee_k (\text{AtLeast}(\{cnot_{k,\vec{e}} \mid \vec{e} \in \vec{E}\}, 1)) \quad (20)$$

$$\bigvee_{k,i} (\text{AtMost}(\{cnot_{k,\vec{e}} \mid q_i \in \vec{e}; \vec{e} \in \vec{E}\}, 1)) \quad (21)$$

F. Constraints for Depth-Based Doubly Optimal

For Depth-Based Doubly Optimal, we incrementally add constraints to reduce the total number of CNOTs after obtaining a depth-optimal solution. We begin by restricting the total number of CNOTs to n_{cnot} using the following constraint:

$$\text{AtMost} \left(\{ \text{cnot}_{k,\vec{e}} \mid \vec{e} \in \vec{E}, k \in [0, K] \}, n_{\text{cnot}} \right). \quad (22)$$

G. Incremental Solving Algorithm for Doubly Optimal

To achieve doubly optimal synthesis, we first optimize one metric (either CNOT count or depth), and then introduce additional constraints to optimize the other. The key difference between CNOT-based and depth-based doubly optimal synthesis lies in the specific constraints required. We categorize them into three types of constraints:

- **Optimal Constraints** (`O_Constraints`) — used to obtain the primary-optimal solution in Step 1.
- **Doubly-Optimal Constraints** (`DO_Constraints`) — used to initialize the secondary optimization in Step 2.
- **Doubly-Control Constraints** (`DC_Constraints`) — applied incrementally to optimize the secondary metric while preserving the base-optimal solution.

We summarize the types of constraints and the specific constraint used in each synthesis in Table I. Algorithm 1 presents our incremental solving procedure for double optimal synthesis.

Algorithm 1 `HOPPS(I, G, T, Θ , CP)`: Incremental Solving for Doubly Optimal Circuit

```

1: Input:  $I$  (initial parity matrix),  $G$  (final parity matrix),  $T$ 
   (parity table),  $\Theta$  (term angles),  $CP$  (coupling map)
2: Output:  $qc$  (optimized quantum circuit)
3: for  $k = n_{\text{term}}$  to  $K_{\text{max}}$  do
4:    $\text{Const} \leftarrow \text{O\_Constraints}(I, G, T, k, CP)$ 
5:    $\text{model.add}(\text{Const})$ 
6:   if  $\text{model.solve}()$  then
7:      $n_{\text{cnot}} \leftarrow \text{model.countCNOTs}()$ 
8:      $s_{\text{model}} \leftarrow \text{model}$ 
9:      $\text{Const} \leftarrow \text{DO\_Constraints}(n_{\text{cnot}})$ 
10:     $\text{model.add}(\text{Const})$ 
11:    for  $n_c = n_{\text{cnot}}$  downto 0 do
12:       $\text{Const} \leftarrow \text{DC\_Constraints}(n_c)$ 
13:       $\text{model.add}(\text{Const})$ 
14:      if  $\text{model.solve}()$  then
15:         $s_{\text{model}} \leftarrow \text{model}$ 
16:      else
17:         $qc \leftarrow s_{\text{model.extract\_circuit}}(\Theta)$ 
18:        return  $qc$ 
19:      end if
20:    end if
21:  end if
22: end for

```

TABLE I: Constraints for Doubly Optimal Synthesis

Constraint Type	CNOT-based	Depth-based
	<code>O_Constraints</code>	Eq. 5, 6, 7, 8, 9, 10 Eq. 11, 12
<code>DO_Constraints</code>	Eq.13 14 15 16 17 18	None
<code>DC_Constraints</code>	Eq. 19	Eq. 22

Constraints defined in Section IV.

V. HOPPS FOR CIRCUIT OPTIMIZATION

A. Peephole Optimization

First, we propose HOPPS can perform peephole optimization for quantum circuit. This idea has been previously explored in works such as [14], [21]. Specifically, we identify subcircuits composed solely of $\{\text{CNOT}, R_z(\theta)\}$ gates as blocks, using HOPPS to synthesize their optimal circuits, and rewrite the original blocks with the optimized versions. HOPPS is flexible in setting different T , G , and CP , making it well-suited for this task.

B. Iterative Blockwise Optimization

However, some blocks may still face scalability problems while optimizing them, especially in circuits like QAOA, which are almost entirely composed of $\{\text{CNOT}, R_z(\theta)\}$ gates. To address this situation, we partition large blocks (circuits) into smaller subblocks (subcircuits), each of which is optimized individually and then reassembled into the circuit.

We observe that, sometimes, a single round of optimization does not yield the maximum possible benefit. Therefore, we apply the optimization iteratively until no further improvement can be achieved. We divide this process into two stages. In the first stage, we partition the entire large block into subblocks and optimize each subblock. The process is repeated until convergence, or until the maximum iteration limit is reached. In the second stage, we randomly sample subblocks within larger blocks and apply optimization to them. This stage is repeated for a fixed number of iterations. The full procedure is described in the Fig. 3.

C. Parallelization

A key advantage of blockwise optimization is that it enables parallel execution of each block independently. Since we are solving a SAT problem, which is inherently suitable for parallelism, we implement a parallel processing strategy where multiple processes are launched, each assigned number of CPUs to enable multithreaded solver execution. Our parallelization approach is illustrated in Step 2 of Fig. 3.

HOPPS relies on a SAT solver, where computational resources are typically the primary limiting factor rather than memory. For the blockwise optimization, blocks are independent of each other and each block is restricted in size. Thus, the problem requires solving multiple controllable SAT problems in parallel and there are no conflicts between solving different blocks. We therefore consider this a computationally bound problem, and providing more CPUs will help accelerate performance.

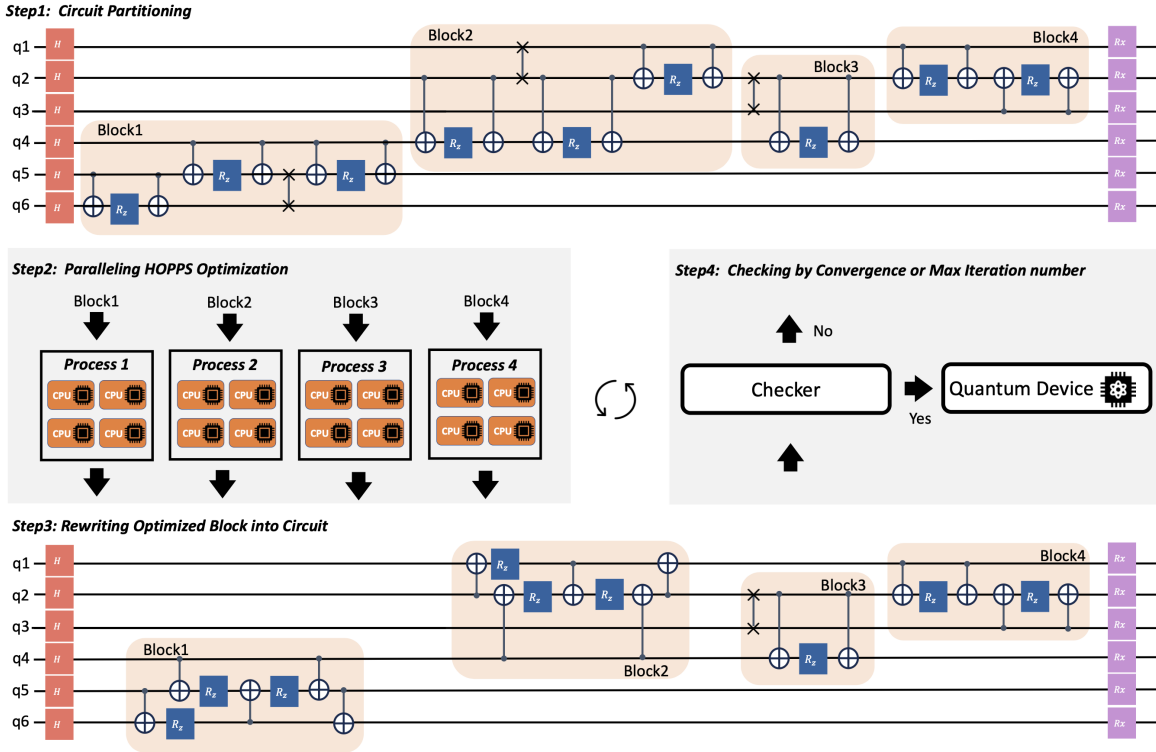


Fig. 3: A pipeline overview of the Blockwise Optimization process: we first partition the circuit into blocks and then apply HOPPS in parallel to optimize each block. Afterward, we track metrics such as CNOT count and CNOT depth to check for convergence. If the circuit has converged, it is compiled for execution on a real device; otherwise, the process is repeated.

VI. RELATED WORK

We review related work from three perspectives: phase polynomial synthesis; blockwise optimization and synthesis; the use of solvers in quantum compilation.

Phase Polynomial Synthesis. Previous studies on phase polynomial synthesis for fault-tolerant circuits focus on minimizing T gates, as these gates introduce substantial overheads [22]–[24]. In the noisy intermediate-scale quantum (NISQ) era, however, CNOT gates become more critical due to their relatively high error rates. Gray-Synth, introduced in [18], was originally designed for synthesizing logical circuits. The work by [21] provides optimal solutions for such logical circuit synthesis. For physical circuits, heuristic approaches have been proposed for synthesizing dense and large parity tables [12], [13]. Inspired by phase polynomial synthesis, [17] introduced the *twin chain* method to map fully connected circuits under various hardware topologies. Building on this idea, [16] proposed a heuristic extension to handle circuits that are not fully connected. None of the existing research guarantees that phase polynomial synthesis is optimal under arbitrary hardware constraints.

Blockwise Optimization and Synthesis. Blockwise strategies are widely used for quantum-circuit optimization and synthesis. Studies have examined blockwise optimization at the logical-circuit level [25], [26]. Other work focuses on hardware-aware re-optimization that respects device topol-

ogy [27], [28]. Nonetheless, runtime and solution quality remain constrained by the efficiency of current resynthesis tools [29], [30]. Recent work [31] could optimize both within blocks and across block boundaries.

Solver-Based Quantum Compilation. Quantum compilation encompasses several aspects: circuit synthesis, mapping, and optimization. For quantum mapping, several studies have focused on using constraint-based methods to achieve optimal mapping. Works such as [19], [32] employ linear integer programming to compute optimal qubit layouts. In contrast, [33]–[35] leverage SAT solvers to address the same problem. Additionally, [21], [36] presents SAT-based approaches for optimally synthesis Clifford circuits and CNOT circuit respectively.

VII. EXPERIMENT

A. Experiment Setup

Backend: In this paper we focus on widely used and publicly accessible quantum hardware provided by IBM. We target the large device `ibm_kyiv`, as well as the small device `ibmq_melbourne`. The `ibm_kyiv` device can be accessed freely through IBM.

Benchmark: For general optimal hardware-mapped circuits, we use benchmark circuits from [33], which were optimally permutation-aware mapped onto `ibmq_melbourne`.

For QAOA-based benchmarks, we use circuits for two types of combinatorial problems: MaxCut and LABS (Low

TABLE II: Evaluation of HOPPS as Peephole Optimization

OLSQ [19] Circuit (Ct\ Dp)	CNOTP [21]			Clifford [36]			HOPPS-CNOT			HOPPS-Depth		
	Ct	Dp	Tm	Ct	Dp	Tm	Ct	Dp	Tm	Ct	Dp	Tm
MaxCut8 E10 (26\16)	26	16	0.2	26	16	2.6	<i>Out of Limit</i>			19	9	97.1
MaxCut7 E9 (24\18)	24	18	0.2	24	18	3.0	<i>Out of Limit</i>			18	8	21.3
MaxCut6 E7 (14\14)	14	14	0.1	14	14	0.2	14	6	36560.6	14	6	3.0
MaxCut5 E7 (20\13)	20	13	0.5	20	13	0.5	14	11	33.0	15	8	3.5
LABS4 (8\7)	8	7	0.2	8	7	0.4	6	5	0.2	6	5	0.1
LABS5 (44\35)	35	28	2.2	35	28	2.4	22	21	1977.7	23	15	47.7
barencotof3 (44\41)	38	36	1.5	37	32	8.2	28	28	2.5	29	26	1.9
barencotof4 (78\70)	74	65	3.4	69	62	14.0	59	49	11.7	60	45	5.4
barencotof5(110\95)	108	94	5.1	97	79	24.0	88	75	19.8	89	68	8.6
mod54 (56\49)	48	40	2.3	39	33	25.6	30	28	102.0	32	24	15.5
modmult55 (131\79)	115	69	13.0	125	75	603.7	106	63	458.9	110	59	16.8
qft4 (105\101)	87	82	5.1	80	75	16.2	72	69	9.9	73	60	10.9
rcadder6 (145\102)	139	100	12.1	128	96	445.9	132	90	15.8	132	89	8.9
tof3 (34\33)	34	31	1.4	34	33	3.9	23	19	2.2	24	17	1.5
tof4 (61\55)	61	53	3.6	55	52	13.6	53	41	27.0	55	37	6.0
tof5 (80\71)	76	68	3.3	69	58	18.5	68	61	10.6	72	53	5.0
vbeadder3 (86\75)	79	67	4.3	72	55	100.8	62	43	25.3	66	39	21.3
Max (%)	20.4	20.0		30.3	32.6		50.0	57.1		47.4	57.1	
Mean (%)	5.9	6.8		10.0	11.1		23.3	30.3		22.3	39.9	

Autocorrelation Binary Sequences), 2-local and 4-local QAOA ansätze. For MaxCut we generate random graphs and regular graphs using the `networkx` library. The label “MaxCut n R m” refers to an n -qubit QAOA circuit for a regular graph of degree m , while “MaxCut n E m” refers to an n -qubit QAOA circuit for a random graph with m edges. For the LABS problem we use instances from [37].

Implementation: All experiments were conducted by using Python, with the Z3 solver used for SAT. For iterative blockwise optimization, we use the `QuickPartitioner` provided in `BQSKit` [38].

The experiments were conducted on an HPC system equipped with Intel(R) Xeon(R) Silver 4216 CPUs @ 2.10 GHz. For the HOPPS versus QSearch comparison, each job was executed on a single compute node with 8 CPUs and 128 GB of RAM. The optimization experiments were run on a single compute node with 32 CPUs and 128 GB of RAM. Parallel tasks were executed using up to 8 logical threads via Python’s `multiprocessing` module.

Comparison: First, HOPPS is a circuit synthesis tool; therefore, we compare it with QSearch [30] from `BQSKit`, another hardware-aware circuit synthesis tool that provides near-optimal solutions. Due to their result is close to optimal, we maintain the same performance in terms of CNOT count and depth, and focus primarily on runtime comparison.

Second, HOPPS supports peephole optimization. We use OLSQ [32], an optimal layout synthesis method, as the baseline. For comparison, we apply two optimal-synthesis-based peephole methods: CNOTP [21] and Clifford [36].

Third, for large-scale $\{\text{CNOT}, R_z(\theta)\}$ circuits, we compare our approach with `BQSKit`’s partition-and-resynthesis strategy, specifically using the `QuickPartitioner` combined with the `QSearchSynthesisPass`. The baseline compilers include `Qiskit`, 2QAN [39], and ArPhase [13]. Among these methods, 2QAN is limited to two-local QAOA circuits only,

whereas ArPhase excels on multi-local circuits but is less effective for two-local instances. Therefore, we would not have 2QAN results for the LABS category, and ArPhase is not reported for the larger MaxCut benchmarks.

Metrics: To compare circuit sizes, we use commonly adopted metrics: **CNOT count** (Ct), which refers to the number of CNOT gates in the circuit, and **CNOT depth** (Dp), defined as the length of the longest path consisting only of CNOT gates. We focus on CNOT depth because, in current quantum devices, two-qubit gates typically have longer durations than do single-qubit gates. A circuit with many single-qubit gates along the critical path should not be considered equivalent in duration to one with many two-qubit gates. Therefore, we argue that CNOT depth is a more appropriate metric for evaluating circuit depth. We compute the improvement ratio as

$$\frac{\text{baseline} - \text{our method}}{\text{baseline}}$$

which reflects the percentage of improvement. To evaluate algorithm efficiency, we also report the **solving time** (Tm) (in seconds).

B. HOPPS as a $\{\text{CNOT}, R_z(\theta)\}$ Peephole Optimization Pass

HOPPS can be applied as a peephole optimization pass on mapped circuits. We use various types of circuits mapped by OLSQ on `ibmq_melbourne` as the baseline. We extract all $\{\text{CNOT}, R_z(\theta)\}$ blocks and perform resynthesis on each block. For QAOA circuits, which are almost entirely composed of $\{\text{CNOT}, R_z(\theta)\}$ operations, HOPPS synthesizes the entire circuit directly. For comparisons, we compare against CNOTP [21]—another peephole optimization method focused on resynthesizing CNOT blocks—and Clifford [36], a peephole optimization method focused on resynthesizing Clifford blocks. The result is presented in the Table II.

Compared with , HOPPS-CNOT reduces the CNOT count up to **50.0%** and the CNOT depth by **57.1%**. HOPPS-Depth achieves average reductions of **23.3%** in CNOT count and **57.1%** in CNOT depth. Across all benchmark circuits, both HOPPS variants outperform CNOTP and Clifford.

C. HOPPS as an Iterative Block Optimization Strategy

For large $\{\text{CNOT}, R_z(\theta)\}$ blocks, we propose an iterative block optimization strategy. We use various types of circuits compiled by Qiskit, 2QAN [39] and ArPhase [13] on `ibmq_kyiv` as the baseline. For comparison, we use an iterative version of BQSKit’s partition-and-resynthesis approach, specifically combining the `QuickPartitioner` with the `QSearchSynthesisPass` in multiple iterations. Since QSearch does not scale beyond 3 qubits, the BQSKit strategy is applied using 3-qubit block partitions. To ensure a fair comparison, we evaluate HOPPS with 3-qubit block partitions and additionally with 5-qubit block partitions to demonstrate its scalability. In some cases, a block becomes too deep; therefore, we cap the maximum block depth at 20. For each circuit, we perform 5 iterations of full-circuit partitioning, followed by 5 iterations sampling blocks. Iterations can be stopped early if no explicit improvement is achieved or out of 24 hours. The result is shown in the Table III.

Using the iterative optimization strategy with HOPPS, we achieving reductions in CNOT count and depth of up to **44.4%** and **42.4%** relative to Qiskit, **11.9%** and **18.1%** relative to 2QAN, and **6.6%** and **9.0%** relative to ArPhase, respectively. Moreover, the iterative optimization strategy that integrates HOPPS surpasses the one built with BQSKit.

We also provide examples that illustrate the benefit of iterative optimization. In Fig. 4a, increasing the number of iterations steadily reduces both the CNOT count and the CNOT depth until they converge. In Fig. 4b, circuits of various sizes achieve larger reductions when optimized multiple times rather than just once.

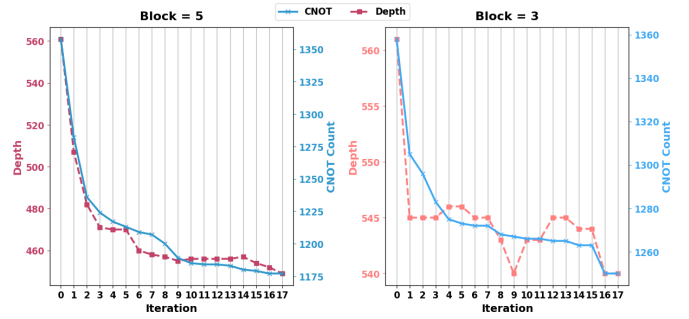
In conclusion, the iterative blockwise optimization strategy is better than perform single-pass, achieving substantial improvements over Qiskit and 2QAN and a slight improvement over ArPhase. This is because ArPhase targets dense parity tables, while the others are SWAP-based compilers. SWAP-based compilers get more chance to be optimized by HOPPS.

D. Runtime Comparison: HOPPS vs. QSearch

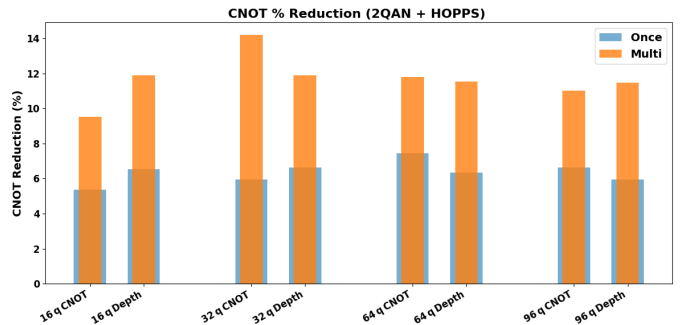
To evaluate HOPPS’s efficiency, we compare its runtime against QSearch in BQSKit. We use small circuits that allow the synthesizer to synthesize the entire circuit directly. These circuits are chosen so that both methods yield identical CNOT counts and depths, ensuring optimality. If the runtime exceeds 2 hours, the result is omitted from the figure. We explore both the runtime scale with the circuit depth and width, and the results are presented in Fig. 5. HOPPS demonstrates better scalability than QSearch with respect to both depth and width.

VIII. DISCUSSION

In this section, we highlight several advantages of HOPPS.



(a) Iteration of CNOT count and CNOT depth for the iterative blockwise optimization on the Qiskit MaxCut 64R4 circuit, optimized by HOPPS-CNOT with different block sizes. We perform 10 iterations of full-circuit partitioning, and 10 iterations sampling blocks.



(b) CNOT reduction rate for multi-pass versus single-pass iterations across 2QAN mapped MaxCut R4-QAOA circuits of varying qubit counts.

Fig. 4: Behavior of Iterative Blockwise Optimization Strategy.

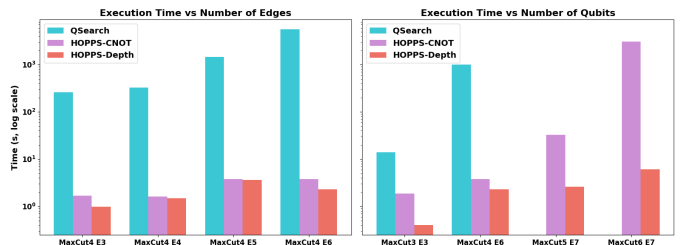


Fig. 5: HOPPS vs. QSearch [30] Synthesis Time. Under equivalent synthesis quality—defined as achieving the same CNOT count and depth—HOPPS requires less execution time compared to QSearch. In the left figure, we fix the number of qubits and vary the number of edges to examine how synthesis time scales with circuit depth. In the right figure, we maintain a similar number of edges while increasing the number of qubits to evaluate scalability with circuit width. The results show that HOPPS is more scalable, particularly depth HOPPS. This demonstrates the advantage of HOPPS for synthesizing $\{\text{CNOT}, R_z(\theta)\}$ circuits.

TABLE III: Evaluation of Iterative Blockwise Optimization Strategy

Compiler	Circuit (Ct\ Dp)	BQSKit (3)			HOPPS-CNOT (3)			HOPPS-Depth (3)			HOPPS-CNOT (5)			HOPPS-Depth (5)		
		Ct	Dp	Tm	Ct	Dp	Tm	Ct	Dp	Tm	Ct	Dp	Tm	Ct	Dp	Tm
Qiskit	MaxCut16 R4 (137\ 79)	127	74	173.8	119	74	21.8	121	73	20.5	111	60	329.4	117	62	35.8
	MaxCut32 R4 (392\ 193)	389	183	176.3	375	185	41.3	372	177	34.9	354	159	687.3	354	146	65.4
	MaxCut64 R4 (1358\ 561)	1285	549	374.7	1286	528	79.3	1267	537	73.1	1185	465	13460.6	1214	467	200.4
	MaxCut96 R4 (2649\ 1086)	2386	891	7086.1	2378	902	421.0	2385	878	206.1	2316	800	78542.4	2288	745	753.4
	LABS20 (12585\ 7459)	10183	5826	1224.0	10079	5683	768.9	10041	5629	529.0	8522	4245	12849.0	8323	4057	695.5
	LABS15 (4128\ 2808)	3234	2176	496.7	3171	2085	248.9	3196	2112	187.5	2594	1490	18018.5	2608	1469	610.5
	LABS10 (875\ 672)	663	513	169.7	637	470	67.8	641	473	55.2	486	311	5476.1	506	318	46.04
	Max (%)	24.2	23.6		27.2	30.0		26.7	29.6		44.4	42.1		37.5	42.4	
Mean (%)	12.6	14.2		14.7	16.0		14.7	16.8		23.9	23.0		19.2	22.1		
2QAN [39]	MaxCut16 R4 (168\ 68)	159	64	83.6	158	63	19.1	157	65	16.4	148	60	2036.4	152	71	65.8
	MaxCut32 R4 (437\ 97)	411	97	148.9	403	93	39.6	403	96	21.4	385	94	2433.1	387	91	71.5
	MaxCut64 R4 (1169\ 209)	1103	208	191.4	1097	205	78.7	1108	201	54.6	1031	171	25417.8	1041	184	232.91
	MaxCut96 R4 (2205\ 262)	2083	262	5928.2	2078	258	166.4	2063	254	102.1	1962	274	62838.1	1952	239	444.1
	Max (%)	5.9	5.8		7.7	7.3		7.7	4.4		11.9	18.1		11.4	11.9	
	Mean (%)	5.6	1.5		6.4	3.7		6.4	3.0		11.6	7.1		10.8	5.6	
ArPhase [13]	MaxCut16 R4 (463\ 274)	461	273	73.2	461	272	17.8	461	272	18.0	448	266	4166.8	450	264	58.0
	MaxCut32 R4 (1949\ 679)	1942	685	41.6	1938	678	154.5	1943	681	17.8	1919	680	155.8	1922	683	98.9
	LABS20 (7218\ 2380)	7210	2384	290.1	7211	2384	236.9	7211	2383	135.9	7107	2375	4749.6	7130	2359	303.1
	LABS15 (2229\ 982)	2207	983	167.7	2213	988	107.2	2214	983	74.1	2146	977	2611.7	2151	971	122.3
	LABS10 (363\ 220)	360	216	111.5	360	216	24.3	360	217	27.5	339	204	461.1	342	200	105.8
	Max (%)	0.9	1.8		0.8	1.8		0.8	1.3		6.6	7.2		5.7	9.0	
Mean (%)	0.5	0.2		0.5	0.3		0.4	0.3		3.3	2.1		2.9	2.0		

“BQSKit (3)” indicates that the circuit is partitioned into 3 qubit blocks using the BQSKit strategy, the same notation is used for the other methods.

Efficiency for QAOA: In QAOA algorithms, parameters are iteratively updated across optimization steps. With methods such as [25], [31], each parameter update requires recompilation and resynthesis of the circuit, which incurs significant overhead. In contrast, HOPPS allows the QAOA circuit to be compiled only once. Subsequent parameter updates can be applied directly to the circuit without recompilation, significantly reducing overall compilation time.

Optimality Checking: After mapping or applying other optimizations to a circuit, it is often beneficial to check whether the $\{\text{CNOT}, R_z(\theta)\}$ subcircuit is optimal. This type of optimality check is not addressed by prior work such as [12], [13]. HOPPS provides a way to verify and improve such blocks, potentially enhancing circuit quality even after traditional compilation flows.

Interoperability. While this paper adopts BQSKit for circuit partitioning, we claim HOPPS can be suitably integrated with other frameworks, such as those proposed in [25], [40].

IX. CONCLUSION AND FUTURE WORK

In this paper, we proposed **HOPPS**: a *Hardware-Aware Optimal Phase Polynomial Synthesis* tool. HOPPS can synthesize $\{\text{CNOT}, R_z\}$ circuits under arbitrary device topologies and provides both CNOT-based and depth-based doubly optimal results (as discussed in Section III-B). Compared to QSearch, HOPPS achieves better runtime performance and scales more effectively with circuit width and depth.

We further demonstrated that HOPPS can serve as a quantum circuit optimizer. For small blocks, it performs direct synthesis; for large blocks—where optimal synthesis becomes intractable—we introduced an iterative blockwise optimization

strategy. We show that modern compilers such as [19], Qiskit, 2QAN [39], and ArPhase [13] can all benefit from HOPPS optimization, outperforming existing optimization strategies. Beyond circuit optimization, HOPPS offers several broader applications:

Template discovery—HOPPS can uncover optimization templates that are difficult for humans to identify manually.

Hardware-aware template design—It can guide the creation of specialized templates for particular topologies, such as QAOA circuits mapped to the *twin chain* architecture [17].

Dataset generation for AI models—HOPPS produces high-quality synthesized circuits that can serve as training data for AI-driven synthesis and optimization tools.

In future work, we plan to integrate HOPPS into end-to-end quantum-compilation pipelines and explore its synergy with learning-based methods.

ACKNOWLEDGMENT

This work was supported in part by the NSF research grant 2216923. This material is based upon work supported by the DOE-SC Office of Advanced Scientific Computing Research MACH-Q project under contract number DE-AC02-06CH11357.

REFERENCES

- [1] G. Q. AI *et al.*, “Quantum error correction below the surface code threshold,” *Nature*, vol. 638, no. 8052, p. 920, 2024.
- [2] D. C. McKay, I. Hincks, E. J. Pritchett, M. Carroll, L. C. Gavia, and S. T. Merkel, “Benchmarking quantum processor performance at scale,” *arXiv preprint arXiv:2311.05933*, 2023.
- [3] C. Monroe, R. Raussendorf, A. Ruthven, K. R. Brown, P. Maunz, L.-M. Duan, and J. Kim, “Large-scale modular quantum-computer architecture with atomic memory and photonic interconnects,” *Physical Review A*, vol. 89, no. 2, p. 022317, 2014.

- [4] D. Bluvstein, H. Levine, G. Semeghini, T. T. Wang, S. Ebad, M. Kalinowski, A. Keesling, N. Maskara, H. Pichler, M. Greiner *et al.*, “A quantum processor based on coherent transport of entangled atom arrays,” *Nature*, vol. 604, no. 7906, pp. 451–456, 2022.
- [5] G. Yan, W. Wu, C. Yuheng, K. Pan, X. Lu, Z. Zixiang, W. Yuhan, R. Wang, and J. Yan, “Quantum circuit synthesis and compilation optimization: overview and prospects,” *CoRR*, 2024.
- [6] J. Kusyk, S. M. Saeed, and M. U. Uyar, “Survey on quantum circuit compilation for noisy intermediate-scale quantum computers: Artificial intelligence to heuristics,” *IEEE Transactions on Quantum Engineering*, vol. 2, pp. 1–16, 2021.
- [7] E. Farhi, J. Goldstone, and S. Gutmann, “A quantum approximate optimization algorithm,” *arXiv preprint arXiv:1411.4028*, 2014.
- [8] F. Orts, G. Ortega, E. F. Combarro, and E. M. Garzón, “A review on reversible quantum adders,” *Journal of Network and Computer Applications*, vol. 170, p. 102810, 2020.
- [9] Y. S. Weinstein, M. Pravia, E. Fortunato, S. Lloyd, and D. G. Cory, “Implementation of the quantum fourier transform,” *Physical review letters*, vol. 86, no. 9, p. 1889, 2001.
- [10] A. Montanaro, “Quantum circuits and low-degree polynomials over \mathbb{F}_2 ,” *arXiv preprint arXiv:1607.08473*, 2016.
- [11] C. M. Dawson, H. L. Haselgrove, A. P. Hines, D. Mortimer, M. A. Nielsen, and T. J. Osborne, “Quantum computing and polynomial equations over the finite field \mathbb{Z}_2 ,” *arXiv preprint quant-ph/0408129*, 2004.
- [12] V. Vandaele, S. Martiel, and T. G. de Brugière, “Phase polynomials synthesis algorithms for NISQ architectures and beyond,” *Quantum Science and Technology*, vol. 7, no. 4, p. 045027, 2022.
- [13] A. M.-v. de Griend and R. Duncan, “Architecture-aware synthesis of phase polynomials for NISQ devices,” *arXiv preprint arXiv:2004.06052*, 2020.
- [14] G. Meuli, M. Soeken, and G. De Micheli, “SAT-based {CNOT, T} quantum circuit synthesis,” in *Reversible Computation: 10th International Conference, RC 2018, Leicester, UK, September 12-14, 2018, Proceedings 10*. Springer, 2018, pp. 175–188.
- [15] T. Peham, L. Burgholzer, and R. Wille, “Equivalence checking of parameterized quantum circuits: Verifying the compilation of variational quantum algorithms,” in *Proceedings of the 28th Asia and South Pacific Design Automation Conference*, 2023, pp. 702–708.
- [16] J. Montanez-Barrera, Y. Ji, M. R. von Spakovsky, D. E. B. Neira, and K. Michielsen, “Optimizing qaoa circuit transpilation with parity twine and swap network encodings,” *arXiv preprint arXiv:2505.17944*, 2025.
- [17] F. Dreier, C. Fleckenstein, G. Aigner, M. Fellner, R. Stahn, M. Lanthaler, and W. Lechner, “Connectivity-aware synthesis of quantum algorithms,” *arXiv preprint arXiv:2501.14020*, 2025.
- [18] M. Amy, P. Azimzadeh, and M. Mosca, “On the CNOT-complexity of CNOT-PHASE circuits,” *arXiv preprint arXiv:1712.01859*, 2017.
- [19] B. Tan and J. Cong, “Optimal layout synthesis for quantum computing,” in *Proceedings of the 39th International Conference on Computer-Aided Design*, 2020, pp. 1–9.
- [20] G. Li, Y. Ding, and Y. Xie, “Tackling the qubit mapping problem for NISQ-era quantum devices,” in *Proceedings of the twenty-fourth international conference on architectural support for programming languages and operating systems*, 2019, pp. 1001–1014.
- [21] I. Shaik and J. van de Pol, “Optimal layout-aware CNOT circuit synthesis with qubit permutation,” in *ECAI 2024*. IOS Press, 2024, pp. 4207–4215.
- [22] M. Amy and M. Mosca, “T-count optimization and Reed–Muller codes,” *IEEE Transactions on Information Theory*, vol. 65, no. 8, pp. 4771–4784, 2019.
- [23] F. J. Ruiz, T. Laakkonen, J. Bausch, M. Balog, M. Barekatin, F. J. Heras, A. Novikov, N. Fitzpatrick, B. Romera-Paredes, J. van de Wetering *et al.*, “Quantum circuit optimization with AlphaTensor,” *URL https://arxiv.org/abs/2402.14396*, 2024.
- [24] A. Kissinger and J. Van De Wetering, “Reducing the number of non-Clifford gates in quantum circuits,” *Physical Review A*, vol. 102, no. 2, p. 022406, 2020.
- [25] M. Weiden, J. Kallor, J. Kubiawicz, E. Younis, and C. Iancu, “Wide quantum circuit optimization with topology aware synthesis,” in *2022 IEEE/ACM Third International Workshop on Quantum Computing Software (QCS)*. IEEE, 2022, pp. 1–11.
- [26] J. Liu, E. Younis, M. Weiden, P. Hovland, J. Kubiawicz, and C. Iancu, “Tackling the qubit mapping problem with permutation-aware synthesis,” in *2023 IEEE International Conference on Quantum Computing and Engineering (QCE)*, vol. 1. IEEE, 2023, pp. 745–756.
- [27] X.-C. Wu, M. G. Davis, F. T. Chong, and C. Iancu, “Reoptimization of quantum circuits via hierarchical synthesis,” in *2021 International Conference on Rebooting Computing (ICRC)*. IEEE, 2021, pp. 35–46.
- [28] —, “Qgo: Scalable quantum circuit optimization using automated synthesis,” *arXiv preprint arXiv:2012.09835*, 2020.
- [29] E. Smith, M. G. Davis, J. Larson, E. Younis, L. B. Oftelie, W. Lavrijsen, and C. Iancu, “Leap: Scaling numerical optimization based synthesis using an incremental approach,” *ACM Transactions on Quantum Computing*, vol. 4, no. 1, pp. 1–23, 2023.
- [30] M. G. Davis, E. Smith, A. Tudor, K. Sen, I. Siddiqi, and C. Iancu, “Towards optimal topology aware quantum circuit synthesis,” in *2020 IEEE International Conference on Quantum Computing and Engineering (QCE)*. IEEE, 2020, pp. 223–234.
- [31] J. Arora, M. Xu, S. Westrick, P. Liu, D. Li, Y. Ding, and U. A. Acar, “Local optimization of quantum circuits (extended version),” *arXiv preprint arXiv:2502.19526*, 2025.
- [32] W.-H. Lin, J. Kimko, B. Tan, N. Bjørner, and J. Cong, “Scalable optimal layout synthesis for nisq quantum processors,” in *2023 60th ACM/IEEE Design Automation Conference (DAC)*. IEEE, 2023, pp. 1–6.
- [33] I. Shaik and J. Van de Pol, “Optimal layout synthesis for deep quantum circuits on nisq processors with 100+ qubits,” *arXiv preprint arXiv:2403.11598*, 2024.
- [34] A. B. Jakobsen, A. B. Clausen, J. van de Pol, and I. Shaik, “Depth-optimal quantum layout synthesis as sat,” *arXiv preprint arXiv:2506.06752*, 2025.
- [35] J. Yang, Y. A. Kharkov, Y. Shi, M. J. Heule, and B. Dutertre, “Quantum circuit mapping based on incremental and parallel sat solving,” in *27th International Conference on Theory and Applications of Satisfiability Testing (SAT 2024)*. Schloss Dagstuhl–Leibniz-Zentrum für Informatik, 2024, pp. 29–1.
- [36] I. Shaik and J. van de Pol, “Cnot-optimal clifford synthesis as sat,” *arXiv preprint arXiv:2504.00634*, 2025.
- [37] R. Shaydulin, C. Li, S. Chakrabarti, M. DeCross, D. Herman, N. Kumar, J. Larson, D. Lykov, P. Minssen, Y. Sun *et al.*, “Evidence of scaling advantage for the quantum approximate optimization algorithm on a classically intractable problem,” *Science Advances*, vol. 10, no. 22, p. eadm6761, 2024.
- [38] E. Younis, C. C. Iancu, W. Lavrijsen, M. Davis, E. Smith, and USDOE, “Berkeley quantum synthesis toolkit (BQSKit) v1,” 04 2021. [Online]. Available: <https://www.osti.gov/biblio/1785933>
- [39] L. Lao and D. E. Browne, “2qan: A quantum compiler for 2-local qubit Hamiltonian simulation algorithms,” in *Proceedings of the 49th Annual International Symposium on Computer Architecture*, 2022, pp. 351–365.
- [40] S. Ping, N. Sathishkumar, W.-H. Lin, H. Wang, and J. Cong, “A high-performance multilevel framework for quantum layout synthesis,” *arXiv preprint arXiv:2505.24169*, 2025.